Computational model of neurodegenerative damage in the olfactory bulb: role of bulb and damage geometry, damage site, and identification of a potential non-invasive marker of early Parkinson's disease onset

J. Kendall Berry[1*&], Daniel L. Cox[1#]

[1]Department of Physics, University of California, Davis, California, USA

[*]Corresponding author
Email: jkberry@ucdavis.edu

[&] Performed the investigation, and primary writing.
[#] Provided initial conceptualization, supervision, and review and editing of the paper.

Computational model of neurodegenerative damage in the olfactory bulb: role of bulb and damage geometry, damage site, and identification of a potential non-invasive marker of early Parkinson's disease onset

J. Kendall Berry*, Daniel L. Cox

Department of Physics, University of California, Davis, California, USA

*Corresponding author, jkberry@ucdavis.edu

Abstract

The olfactory bulb (OB) is one of the first regions of the brain affected by Parkinson's disease (PD) as measured by both dysfunction and presence of α-synuclein aggregation. Better understanding of how PD affects OB function could lead to earlier diagnosis and potential treatment. By simulating damage to the OB in a computational model, it may be possible to identify regions of interest or markers of early disease. We modified a simple rate-based computational model of the olfactory bulb and simulated damage to various components of the network. This was done for several configurations of the network, at different sizes and with 1D and 2D connectivity structures. We found that, in almost every case, activity of 2D networks were more robust to damage than 1D networks, leading us to conclude that a connection scheme of at least 2D is vital to computational modeling of the OB. We also found that certain types of damage (namely, seeded damage to the granule cell layer and to the synapses between mitral and granule cells) resulted in a peak of the oscillatory power of the network as a function of damage. This result is testable experimentally and bears further investigation utilizing more sophisticated computational models. If proven accurate, this rise in oscillatory power in the OB has the potential to be an early marker of PD.

Author summary

One of the first symptoms of Parkinson's disease is the degradation of the sense of smell. The olfactory bulb is the first region of the brain to process odor information and is affected by Parkinson's disease at early stages. We simulated neural activity in a computational model of the olfactory bulb in the presence of damage and compared it to simulations of undamaged activity. We found that 2D model networks were more robust to damage than their 1D counterparts. We also found that 2D networks displayed increased oscillatory activity when damage was applied to certain parts of the network. This last result, if proven correct, would potentially be a marker of early-stage Parkinson's disease, and if so, could aid in early diagnosis and treatment of the disease.

Introduction

Parkinson's disease (PD) is a neurological disorder affecting over half a million people in North America alone [1], characterized by motor and non-motor symptoms, which include tremors, constipation, sleep disturbances, and olfactory loss [2]. Finding good

early stage markers of pathology and symptoms can facilitate earlier diagnosis and thus result in significantly better care and treatment [3]. Indeed, one of the first symptoms to appear, in most cases before motor symptoms, is loss of olfaction [4, 5], with deficits in odor detection threshold, discrimination, and identification [6–8]. Additionally, aggregates of misfolded α-synuclein, the protein complexes most implicated in PD, are found in the olfactory system early on in the disease [5, 9–11]. In one example, a longitudinal study of elderly Hawaiians showed a mean onset of about 4 years between the onset of olfactory loss and PD onset [12]. Studies like these have led some to propose that the accumulation of misfolded α-synuclein aggregates may begin in the olfactory bulb and propagate from there [9, 13, 14]. Importantly, if olfaction deficits can be positively attributed to PD in the early stages, the possibility of using small molecule protein aggregation inhibitors that cross the blood-brain barrier like anle138b could be deployed to prevent disease [15–17].

The olfactory bulb (OB) is the first processing area for incoming odor information [18]. Odorant molecules bind to olfactory receptors on olfactory receptor neurons, which send their signal to the glomeruli, which are roughly spherical bundles of dendrites located inside the exterior layer of the olfactory bulb [19]. The dendrites belong to a number of neurons, including mitral cells, external tufted cells, short axon cells, and periglomerular cells [19]. The mitral and external tufted cells send their excitatory signals to olfactory cortical regions. They also excite the interneurons of the OB, called granule cells, which in turn inhibit the mitral cells through graded dendrodentritic interactions [20]. This mix of inhibitory and excitatory interactions drives oscillatory behavior in the OB network in the gamma band (40-80 Hz) [21].

While the odor identity is first encoded in the OB, exactly how it is represented is an ongoing question for which there are various theories, mainly revolving around combinatorics of glomerular or mitral cell activity [22–25]. Oscillations in neural activity in the bulb may also play a part in encoding odor identity, and are likely important to odor recognition or information transfer, or both [21]. The precise manner in which PD impacts OB function is still a matter of investigation [26, 27], although misfolded α-synuclein is present in the mitral, external tufted, granule, and periglomerular cells of PD patients [5, 28, 29].

It remains unclear how α-synuclein aggregates lead to neurodegenerative damage, although a likely candidate for early cellular damage is disruption of transport along the microtubule bundles of the axon with subsequent presynaptic degradation [30–36].

There have been few investigations of the impact of damage that might arise from neurodegeneration or lesions on neural networks, and most have examined the effect on the classical Hopfield model of associative memory, in particular how memory capacity is affected [37–39]. One paper examined how compensation could retain capacity in such an associative memory model [40]. Importantly, we are not aware of any works on biologically plausible sensory neural networks that examine the impact of neurodegenerative damage with an intention towards guiding early diagnosis of the diseases.

We investigate here the impact of neurodegenerative damage on various constituents of a computational model of the OB network. Many excellent and insightful computational models of the OB exist [41], focusing on various aspects of the olfactory system, such as generating oscillatory behavior [42–44], glomerular layer computations [45], and odor computations and representation [24, 46]. As a simple model of the olfactory bulb network-level activity that captures the oscillatory activity in the gamma band [47], we chose to work with the Li-Hopfield model [42]. It simplifies the OB to a network (with periodic boundary conditions) of mitral cells and granule cells (the primary neuronal interaction in the bulb) (see Fig 1A). These cell types are also of particular interest because some studies suggest that mitral and granule cells

may be especially vulnerable to damage in PD [9, 29].

The original Li-Hopfield work generated gamma band oscillations using a one-dimensional network with ten mitral and ten granule cells, with an assertion that similar behavior can be found with a two-dimensional network, and an implication that the behavior was similar for larger networks. In fact, as we show here, the normal behavior of a two-dimensional network is generally more robust against the model damage as measured by how the odor representation diverges from the undamaged case, and also shows, for some types of damage, a significant enhancement of gamma band oscillatory power with increased damage. Because the real mitral-granule layers in the olfactory bulb are two-dimensional, this represents an important difference between the one-dimensional and two-dimensional versions of the model. In particular, we find that damage at the synaptic interface or internal damage to the granule cells lead to enhanced gamma band oscillatory power and a change in odor-evoked response pattern at relatively larger levels of damage. In contrast, damage to the odor inputs or internal damage to the mitral cell inputs lead to reduced oscillatory power with damage but shows a similar modification of the odor-evoked response with damage in two-dimensions. In one-dimension, no matter what the region of damage, typically the gamma band oscillatory power drops with damage, and the odor representation diverges from the undamaged one more quickly than in two-dimensions.

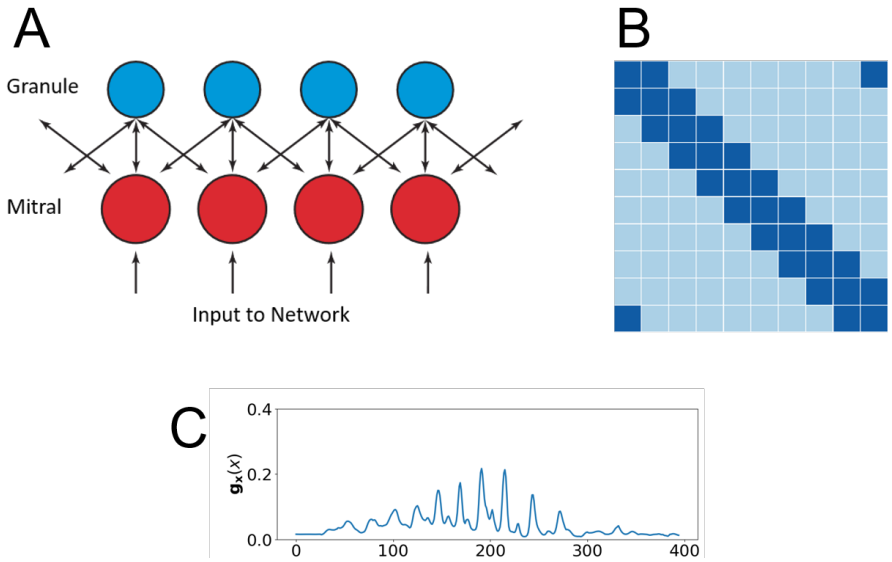

Fig 1. Li-Hopfield Model. A: Mitral cell units receive odor input (via glomeruli, not modeled here) and excite the granule cell units, which in turn inhibit the mitral cell layer. The connections between mitral and granule cell units define a 1D ring structure. The networks implemented here have 20 units (mitral plus granule), 40 units, and 100 units. B: Example weight matrix defining a 1D periodic network. Light blue entries are zero (no connection), dark blue signifies positive non-zero entries (established connection). C: Example of mitral cell output ($\mathbf{g_x}$) over the course of a single inhale-exhale cycle. The inhalation peaks at 205 ms, at which point the exhale begins. Each mitral or granule cell unit should be considered as representing a particular population of mitral cells.

Materials and methods

Li-Hopfield Model

The Li-Hopfield model describes the internal state (representative of membrane potential) and output state (or cell activity, representative of firing rate) of mitral and granule cells over an inhale-exhale cycle. It is governed by the following set of equations,

$$\dot{\mathbf{x}} = -H_0\ \mathbf{g_y}(\mathbf{y}) + \mathbf{I_b} + \mathbf{I_{odor}}(t) - \alpha\mathbf{x}$$
$$\dot{\mathbf{y}} = W_0\ \mathbf{g_x}(\mathbf{x}) + \mathbf{I_c} - \alpha\mathbf{y},$$

where $\mathbf{x}$ and $\mathbf{y}$ are vectors containing the internal state of each mitral cell and each granule cell, respectively (in actuality, each mitral and granule cell should be considered to represent a population of mitral or granule cells). The functions $\mathbf{g_x}$ and $\mathbf{g_y}$ are sigmoidal activation functions [42] that translate internal state into output state, $\mathbf{I_b}$ is tonic uniform background excitatory input to the mitral cells, $\mathbf{I_c}$ is tonic uniform excitatory centrifugal input to the granule cells, and α is the decay constant, which is taken to be the same for mitral and granule cells in this model. Random noise is added to $\mathbf{I_b}$ and $\mathbf{I_c}$ in the form given in the original Li and Hopfield paper [42]. $\mathbf{I_{odor}}$ is the odor input (i.e., glomerular excitation), which rises linearly with inhale and falls exponentially with exhale. $\mathbf{I_{odor}}$ could in principle have different levels of input for each mitral cell. In the simulations here, we defined it to be uniform for simplicity and because damage should affect all odors. H_0 and W_0 are the matrices that define the connections from granule to mitral cells and from mitral cells to granule cells, respectively. The exact functions and values for the parameters can be found in S1 Table.

The connection matrices H_0 and W_0 dictate the structure of the network. The original Li-Hopfield model contained 10 mitral cells and 10 granule cells, connected in mitral-granule pairs, with each pair connecting to neighboring pairs on a 1D ring (Fig 1 A, B). For our work here, we adapted the network to include larger numbers of mitral and granule cells. This was accomplished by initializing a matrix of the desired size with entries of the same order magnitude as the original Li-Hopfield matrices, and then updating the non-zero entries randomly until the desired behavior was achieved. Because the interface between the dendrites of the mitral and granule cells, the external plexiform layer, lies on the surface of an ellipsoid, we also found matrices with 2D architecture for each size in the same way (Fig 2). Therefore, we implement the model in six different architectures: 20 cells (mitral plus granule), 40 cells, and 100 cells in 1D and 2D. It should be noted that W_0 in the original Li-Hopfield model included extra connections that make the architecture not truly 1D. These connections have been retained for the 1D 20 cell network, but are not present in any of the other 1D network structures. The specific matrices for each size can be found on the Github repository (see Supporting Information). As noted in Ref. [42], the equal numbers of mitral and granule cells in the network is not realistic; there are approximately 200 times more granule than mitral cells. Exploration of the effects of this difference is beyond the scope of the present paper.

Damage

By taking a computational model of the olfactory bulb and perturbing the network, we can make predictions regarding the impact of various types of damage. The simulations are run in Python using Scipy's solve_ivp function [48], and all code for the simulations can be found on the Github repository (see Supporting Information). Damage to the

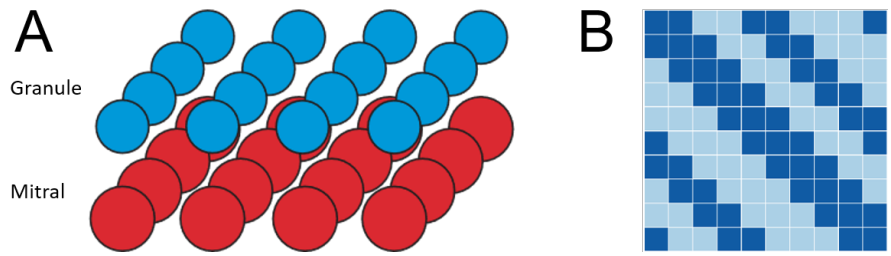

Fig 2. 2D Model. A: The connections between mitral and granule cell units are largely the same as in 1D, but extend in two directions. B: Example of a weight matrix structure defining a 2D periodic network structure. Light blue entries are zero (no synaptic connection), dark blue signifies positive non-zero entries (established synaptic connection). Each mitral (granule) cell connects to its granule (mitral) pair, as well as four other granule (mitral) cells.

network is measured by δ, the fraction of weight removed. For the weight matrices, W_0 for example,

$$\delta = 1 - \frac{\sum_{ij} W_{Damaged,ij}}{\sum_{ij} W_{0,ij}},$$

where W_0 is the undamaged matrix and $W_{Damaged}$ is the damaged matrix. In a given trial, damage is delivered to one of the following components of the model:

- W_0, the synaptic connections from mitral to granule cells
- H_0, the synaptic connections from granule to mitral cells
- Granule cell layer
- Mitral cell layer
- $\mathbf{I_{odor}}$, the input to mitral cells from the glomerular layer

Internal damage to the mitral cell layer (MCL) or to the granule cell layer (GCL) is implemented by multiplying the right-hand-side of the differential equation (except for the leak term) for the given cell by some fraction less than one, $(1 - \delta_i)$. For example,

$$\dot{x}_i = (1 - \delta_i)(-\sum_j H_{0,ij}\ g_{y,j}(y_j) + I_{b,i} + I_{odor,i}(t)) - \alpha\ x_i$$

would be damage delivered to the ith mitral cell unit. In this case, δ is calculated as

$$\delta = \sum_i \frac{\delta_i}{N},$$

where N is the number of mitral cells.

We ramp up the damage to the selected part of the network, run the network at that damage level, and compare the activity to the activity of the undamaged network. The damage is propagated in one of three ways: Flat Damage (FD), Columnar Damage (CD), or Seeded Damage (SD).

For FD, the damage is delivered to every element of the selected component equally. This amounts to simply scaling the chosen quantity uniformly. For example, if FD was applied to H_0, each element of H_0 would be reduced by the same fraction of its original

value on each damage step. This continues until the matrix is reduced to zero (see Fig 3 A).

For CD, the damage is delivered to a specific element (or column if the network quantity is a matrix), ramped up until that element is reduced to zero, and then that procedure is repeated on an adjacent element until the maximum damage level is reached. For example, if CD was delivered to H_0, damage would be delivered incrementally to a single column (i.e., the postsynaptic strength of a single granule cell) until it was reduced to zero. The same process would then begin on the column to the right (see Fig 3 B). We continue this process until 50% of the columns are removed.

SD is a combination of FD and CD. Damage is first delivered to a single element (or column), and on the next damage step, damage is delivered to that element again, as well as to neighboring elements. For example, if SD was enacted on H_0 in a 1D network, it would begin on one column, say column 6. On the subsequent damage step, the damage would be delivered to columns 5, 6, and 7. This spreading continues with each damage level until the matrix is reduced to zero (Fig 3 C).

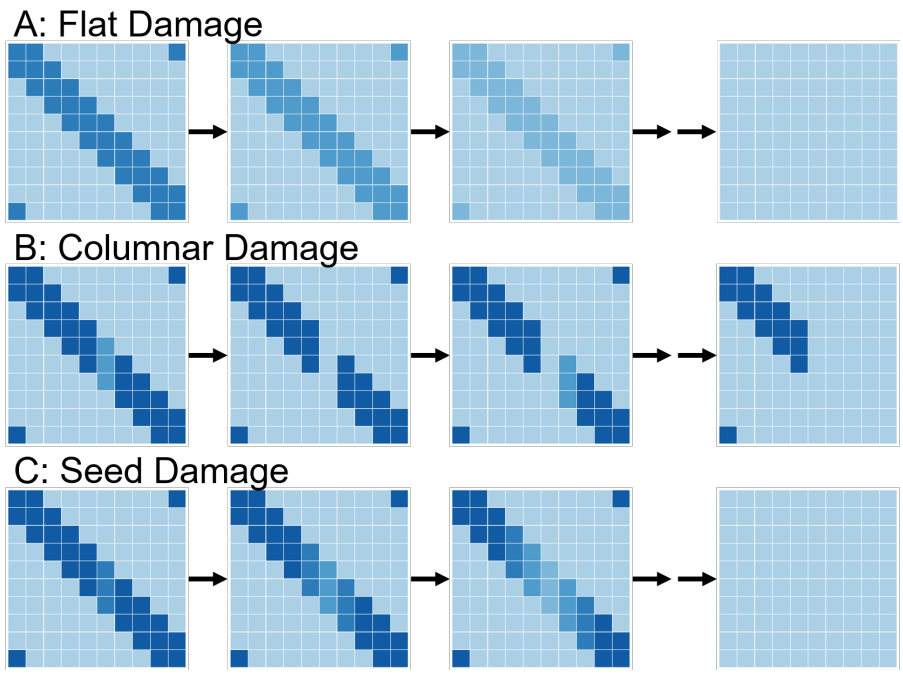

Fig 3. Schematic of Damage Propagation Strategies. A: Example of FD delivered to H_0 or W_0 in the 1D 20 unit network. B: Example of CD delivered to H_0 or W_0 in the 1D 20 unit network. Damage begins in a single column (in this case, column 6). For CD, we only removed up to half the matrix weight because in most cases, the network activity was already greatly disrupted by that point, and it required a greater number of damage steps. C: Example of seeded damage delivered to H_0 or W_0 in the 1D 20 unit network. Damage begins in a single column (in this case, column 6).

Characterizing Network Activity

We characterize the damaged network's activity by comparing its activity pattern, average activity level, and average oscillatory power to that of the undamaged network.

The activity pattern is measured by low-pass filtering the cell activity and averaging over time for each mitral cell [42]. This yields a response vector **R**, where each entry

reflects the average activity level for a single mitral cell unit. We then compare the response vector for the damaged network, $\mathbf{R_D}$, with the response vector for the undamaged network, $\mathbf{R_0}$, by calculating the distance between activity patterns, D_P [42]:

$$D_P = 1 - \frac{\mathbf{R_D} \cdot \mathbf{R_0}}{|\mathbf{R_D}||\mathbf{R_0}|}.$$

This normalizes the maximum distance between patterns to $D_P = 1$, with identical patterns giving $D_P = 0$. If D_P increases with damage level, that indicates that the damaged network's activity pattern for a given odor input is diverging from that of the undamaged network.

The average activity level, $\overline{R}$, is calculated as a root-mean-square of the response vector $\mathbf{R}$. We measure the difference between average activity levels, D_A, by [42]:

$$D_A = \frac{\overline{R_D} - \overline{R_0}}{\overline{R_D} + \overline{R_0}},$$

which has a max of $|D_A| = 1$ and a min of $|D_A| = 0$. We retain the sign in practice because it indicates whether the average activity level of the damaged network is greater or less than the null case.

We calculate the average oscillatory power, P_{avg}, by first high-pass filtering the mitral cell activity above 15 Hz to ignore theta band (2-12 Hz) activity, which was beyond the scope of the present study. We next calculate the power spectrum ($\mathbf{P}(f)$) for each mitral cell from 125 ms to 250 ms using Scipy's periodogram function [48]. This time window captures the oscillatory behavior during the most active part of the cycle (see 1C) while ignoring the spurious signals that can arise at higher levels of damage that are not actually due to gamma band oscillatory activity (see S10 Fig). We then integrate the power spectrum over all frequencies, f, for each cell (see S10 Fig) and average over the mitral cell population (N) to get P_{avg}.,

$$P_{avg} = \frac{1}{N} \sum_{i=1}^{N} \int_0^\infty P_i(f) df.$$

Each quantity is averaged over five trials. For CD and SD, we then repeat the trial using each cell as the starting point and average the values again over all starting cells.

Results

Damage to W_0, H_0, and GCL

CD caused network activity to diverge from the undamaged case at the lowest δ, followed in impact as a function of δ by SD and FD respectively, as shown in Fig 4. This was consistent across network sizes and structures for damage delivered to W_0, H_0, and GCL (see S1 Fig - S6 Fig).

The 2D networks were more robust than their 1D counterparts in almost every case, as measured by how quickly their activity diverged from the undamaged case (Fig 5). This is especially apparent in SD delivered to W_0, H_0, and GCL, but can also be seen in CD and FD for those neuronal regions (S1 Fig - S6 Fig).

The effect of damage on average oscillatory power also depended on the damage scheme and network structure. FD and SD in 2D networks resulted in increases in P_{avg} at intermediate δ (Fig 6A), but CD rarely showed an increase in P_{avg} (S8 Fig). While this rise in P_{avg} was ubiquitous among 2D networks with FD and SD, P_{avg} decreased monotonically for most 1D cases (see Fig 6B).

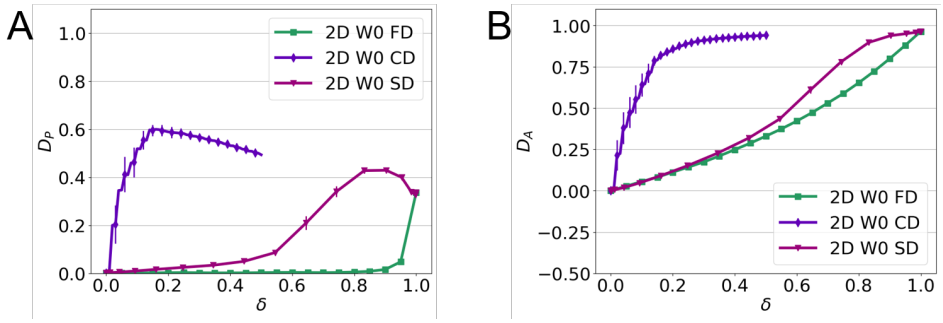

Fig 4. Flat, Columnar, and Seeded Damage Compared. A: Distance in activity pattern (D_P) for FD, CD, and SD delivered to the connection matrix W_0 in the 2D 100 cell network plotted against damage as a fraction of total synaptic weight removed (damage level, δ). The activity pattern diverges from the undamaged case most quickly in CD, as indicated by the rapid rise in D_P. B: Distance in average activity level (D_A) for FD, CD, and SD delivered to the connection matrix W_0 in the 2D 100 cell network. Like the activity pattern in A, the average activity level diverges from the undamaged case most quickly for CD.

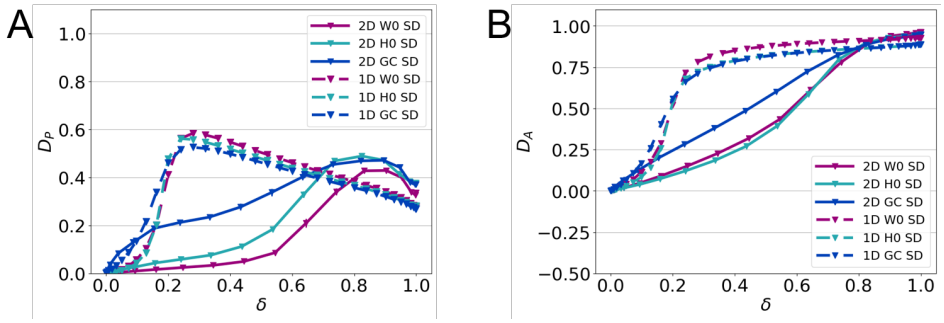

Fig 5. 2D Network Compared to 1D Network, Seeded Damage to W0. A: Distance in activity pattern for SD delivered to W_0, H_0, and GCL in the 1D and 2D 100 cell networks plotted against damage as a fraction of total synaptic weight removed (damage level, δ). In each case, D_P increases to its maximum value most rapidly for the 1D network, indicating a greater divergence from the activity pattern in the undamaged case at lower levels of damage. B: Distance in average activity level for SD delivered to W_0, H_0, and GCL in the 1D and 2D 100 cell networks. In each case again, the 2D network activity is more robust to damage.

Damage to Mitral Cell Layer and Olfactory Input

Trials with damage delivered to MCL and to OI showed qualitatively similar results. Like the W_0, H_0, and GCL trials, network activity patterns were most sensitive to CD, followed respectively by SD and FD (Fig 7A). However, the average activity level changed at a similar rate for all types of damage propagation, though usually most slowly for CD (Fig 7B). Additionally, P_{avg} decreased in every case at similar rates (Fig 7C).

Discussion

The work described here illustrates the importance of the 2D network structure of the OB in terms of robustness against neurodegenerative damage (relative to 1D models),

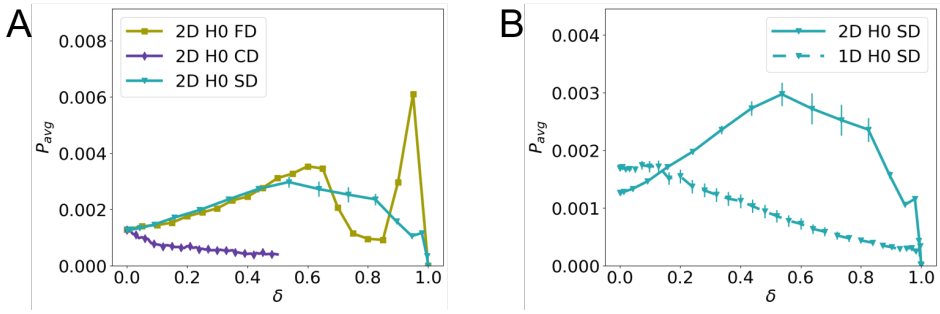

Fig 6. Effect on Oscillatory Power. A: Average oscillatory power (P_{avg}) for FD, CD, and SD delivered to H_0 in the 2D 100 cell network plotted against damage as a fraction of total synaptic weight removed (damage level, δ). B: P_{avg} for SD delivered to H_0 in the 1D and 2D 100 cell networks. FD and SD to H_0 result in a rise in P_{avg} for the 2D network, while CD to the 2D network and any kind of damage to the 1D network do not.

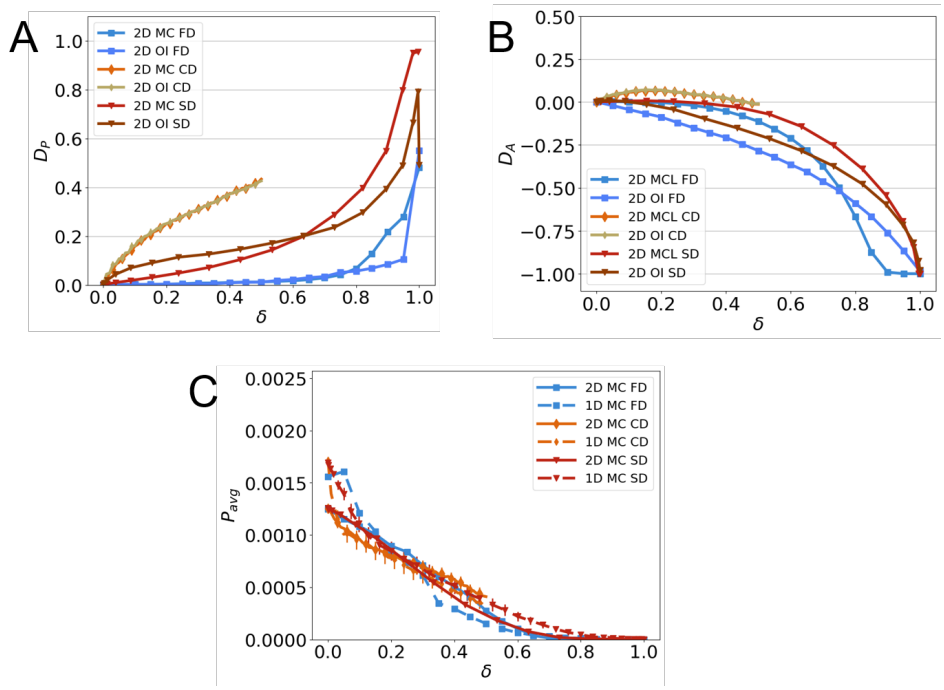

Fig 7. Effects of Damage to Mitral Cells or to Olfactory Input A: Distance in activity pattern for FD, CD and SD delivered to MCL and OI in the 2D 100 cell network plotted against damage as a fraction of total synaptic weight removed (damage level, δ). B: Distance in average activity level for FD, CD and SD delivered to MCL and OI in the 2D 100 cell network. As opposed to damage to W_0, H_0, or GCL, average activity level very nearly decreases monotonically for all cases, with the exception of CD. C: Average ocillatory power for FD, CD, and SD delivered to MCL in the 2D 100 cell network.

as well as in modification of the power spectrum with damage. Computational models of the olfactory bulb have synaptic connection schemes that are mainly either 2D or 3D (for example, [44, 46, 49]), or random (for example, [43, 50]) in structure. We confirm that for applicability to disease models, accounting for the geometric structure of the

bulb is important, as even in the simplistic model implemented here there was a sizeable difference in response to damage based on the dimensionality and geometry of the connection scheme.

The structure of the synaptic connections also has implications for the spread of pathology. We propagated damage here in three ways, FD, CD, or SD. FD and CD represent the two extremes of damage propagation (FD completely delocalized to every cell, and CD completely localized to a single cell before spreading). Misfolded α-synuclein spreads from cell to cell before cell death [51, 52] in what many believe is a prion-like manner [7, 13, 53], although the precise mechanism and the level of damage in the donor cell before transmission is still under investigation [54, 55]. This means the damage would spread differently for a 1D connection scheme compared to 2D. It also makes the SD method the most relevant form of propagation presented here, though FD and CD are still important for comparison.

The results presented above imply that localized damage may be more severe than dispersed damage at similar levels as measured as a fraction of synaptic strength, though some experimental results do not support this [56]. This may be a failing of the model, and taking the plasticity of the bulb into account would likely alter these results.

The work here also illustrates a differentiation between two general groups of damage types. Assuming SD is the most realistic propagation strategy, damage to H_0, W_0, and GCL all result in increased network activity and a peak with damage in gamma band oscillatory power, while damage to MCL and OI do not. This gives specific differentiating factors that can be measured.

One of the most salient results presented here is the peak in P_{avg} for SD to W_0, H_0, and GCL for 2D networks. This provides a testable marker that can help to identify potential network components damaged in PD. In fact, Kulkarni et al. [27] recently recorded local field potentials in mice olfactory bulbs after injection of α-synuclein pre-formed fibrils. They saw a rise in oscillatory power during odor presentation after in incubation period ranging from 1-3 months post-injection. This increase in oscillatory power was in the beta band only (15-30 Hz), while this network models activity in the gamma band (40-80 Hz), so comparison is limited. However, beta oscillations are likely mediated by the same synapses in the OB as gamma [57, 58], and we believe these results to be related. Taken together, they imply PD may damage the synapses between the MCL and the GCL (in this model, W_0 and H_0), although generalized damage to the GCL shows similar results here. Studies have shown that α-synuclein plays a role in synaptic transmission [59, 60], and that α-synuclein oligomers and aggregates disrupt synaptic function [59, 61–63]. Additionally, there is evidence that neurodegeneration in PD may be due to synapse dysfunction rather than just cell death [64]. Therefore, we believe the W_0 and H_0 results to be the most interesting. They are particularly intriguing since a recent study has shown that it is possible to measure such an increase in oscillatory power without an invasive probe to the brain [65], so this can be regarded potentially as a unique early onset marker of the disease.

Opportunities exist for experiments to investigate the results and claims presented here. More acute measurements of olfactory bulb oscillatory activity early on in pre-formed fibril seeding before severe cell damage has a chance to occur could help illuminate whether effects are due to synaptic dysfunction or cell death and could lead to more directed studies in the future.

The model employed here is simplistic. Repeated trials using more biophysically relevant models of the olfactory bulb should be performed. For example, future work should implement a model with activity in both the gamma and the beta bands, such as in models by Osinski & Kay [50] and David [66], requiring more sophisticated centrifugal inputs [57]. Comparing responses to damage across models can uncover commonalities and make reasonable predictions about actual pathology and behavior in

vivo, leading to tools for treatment and early detection.

Conclusion

Taken together with recent work by Kulkarni et al. [27], these results indicate that damage to the synapses between mitral and granule cells could be a potential mechanism (broadly speaking) for olfactory dysfunction in PD. More work needs to be done in looking at this increase in oscillatory power, and a computational model that includes beta oscillation needs to be implemented. Opportunities for both experimental and computational work regarding the results presented here bear further investigation. If the increase in oscillatory power in the presence of pathology is consistently demonstrated, it has the potential to be an early marker of disease. Hopefully by better understanding the impact of damage on olfactory bulb network behavior, we can take steps toward better tools for the early diagnosis for Parkinson's disease.

Acknowledgments

We acknowledge useful conversations with D. Wesson, and A. Kulkarni, and we thank them for critical readings of the manuscript. This grew from preliminary work on the problem by Avinash Baidya, and we thank him for useful discussions about the project.

Supporting information

All code for the simulations can be found at https://github.com/jkberry07/OB_PD_Model.

S1 Table contains the equations and parameters used in the equation. For more information about the parameters, and for information about the noise added to the system, see the original paper by Li and Hopfield [42], as well as Li's dissertation [67].

S1 Fig through S9 Fig show all results for D_P, D_A, and P_{avg} for each type of damage to each part of the network for each network size and structure.

S10 Fig shows an example of cell activity at various δ during SD delivered to W_0 in the 2D 100 unit network. S11 Fig also shows cell activity at various δ and demonstrates an example of what can cause the spike in P_{avg} observed at higher δ in FD H_0 trials.

Supplemental tables and figures are located after the references.

References

1. Marras C, Beck JC, Bower JH, Roberts E, Ritz B, Ross GW, et al. Prevalence of Parkinson's disease across North America. npj Parkinson's Disease. 2018;4(1):21. doi:10.1038/s41531-018-0058-0.

2. Jankovic J. Parkinson's disease: clinical features and diagnosis. Journal of Neurology, Neurosurgery & Psychiatry. 2008;79(4):368. doi:10.1136/jnnp.2007.131045.

3. Murman DL. Early treatment of Parkinson's disease: opportunities for managed care. Am J Manag Care. 2012;18(7 Suppl):S183–8.

4. Ponsen MM, Stoffers D, Booij J, van Eck-Smit BLF, Wolters EC, Berendse HW. Idiopathic hyposmia as a preclinical sign of Parkinson's disease. Annals of Neurology. 2004;56(2):173–181. doi:10.1002/ana.20160.

5. Doty RL. Olfactory dysfunction in Parkinson disease. Nature Reviews Neurology. 2012;8(6):329–339. doi:10.1038/nrneurol.2012.80.

6. Haehner A, Hummel T, Reichmann H. Olfactory loss in Parkinson's disease. Parkinson's disease. 2011;2011:450939–450939. doi:10.4061/2011/450939.

7. Rey NL, Steiner JA, Maroof N, Luk KC, Madaj Z, Trojanowski JQ, et al. Widespread transneuronal propagation of α-synucleinopathy triggered in olfactory bulb mimics prodromal Parkinson's disease. The Journal of experimental medicine. 2016;213(9):1759–1778. doi:10.1084/jem.20160368.

8. Johnson ME, Bergkvist L, Mercado G, Stetzik L, Meyerdirk L, Wolfrum E, et al. Deficits in olfactory sensitivity in a mouse model of Parkinson's disease revealed by plethysmography of odor-evoked sniffing. Scientific Reports. 2020;10(1):9242. doi:10.1038/s41598-020-66201-8.

9. Sengoku R, Saito Y, Ikemura M, Hatsuta H, Sakiyama Y, Kanemaru K, et al. Incidence and Extent of Lewy Body-Related α-Synucleinopathy in Aging Human Olfactory Bulb. Journal of Neuropathology & Experimental Neurology. 2008;67(11):1072–1083. doi:10.1097/NEN.0b013e31818b4126.

10. Braak H, Tredici KD, Rüb U, de Vos RAI, Jansen Steur ENH, Braak E. Staging of brain pathology related to sporadic Parkinson's disease. Neurobiology of Aging. 2003;24(2):197–211. doi:https://doi.org/10.1016/S0197-4580(02)00065-9.

11. Braak H, Ghebremedhin E, Rüb U, Bratzke H, Del Tredici K. Stages in the development of Parkinson's disease-related pathology. Cell and Tissue Research. 2004;318(1):121–134. doi:10.1007/s00441-004-0956-9.

12. Ross GW, Petrovitch H, Abbott RD, Tanner CM, Popper J, Masaki K, et al. Association of olfactory dysfunction with risk for future Parkinson's disease. Annals of Neurology. 2008;63(2):167–173. doi:10.1002/ana.21291.

13. Rey NL, George S, Steiner JA, Madaj Z, Luk KC, Trojanowski JQ, et al. Spread of aggregates after olfactory bulb injection of α-synuclein fibrils is associated with early neuronal loss and is reduced long term. Acta neuropathologica. 2018;135(1):65–83. doi:10.1007/s00401-017-1792-9.

14. Doty RL. The olfactory vector hypothesis of neurodegenerative disease: Is it viable? Annals of Neurology. 2008;63(1):7–15. doi:10.1002/ana.21327.

15. Levin J, Wagner J, Ryazanov S, Leonov A, Shi S, Schmidt F, et al. Causal therapy of Parkinson's disease with anle138b, a novel protein aggregation inhibitor. Movement Disorders. 2011;26:S21–S21.

16. Antonschmidt L, Dervisoglu R, Ryazanov S, Leonov A, Wegstroth M, Giller K, et al. The Small Molecule anle138b Shows Interaction with alpha-Synuclein Oligomers in Phospholipid Membranes. Biophysical Journal. 2018;114(3):560A–560A. doi:10.1016/j.bpj.2017.11.3064.

17. Antonschmidt L, Dervisoglu R, Ryazanov S, Leonov A, Wegstroth M, Giller K, et al. Protein-Drug Interactions in the Membrane: The Small Molecule Anle138b and its Binding to alpha-Synuclein Oligomers. Biophysical Journal. 2019;116(3):352A–352A. doi:10.1016/j.bpj.2018.11.1913.

18. Mori K, Nagao H, Yoshihara Y. The Olfactory Bulb: Coding and Processing of Odor Molecule Information. Science. 1999;286(5440):711. doi:10.1126/science.286.5440.711.

19. Shepherd GM. The synaptic organization of the brain. 5th ed. Oxford ; New York: Oxford University Press; 2004. Available from: `Tableofcontentsonlyhttp://www.loc.gov/catdir/toc/fy043/2003042914.html`.

20. Schoppa NE, Kinzie JM, Sahara Y, Segerson TP, Westbrook GL. Dendrodendritic inhibition in the olfactory bulb is driven by NMDA receptors. The Journal of neuroscience : the official journal of the Society for Neuroscience. 1998;18(17):6790–6802. doi:10.1523/JNEUROSCI.18-17-06790.1998.

21. Kay LM, Beshel J, Brea J, Martin C, Rojas-Líbano D, Kopell N. Olfactory oscillations: the what, how and what for. Trends in neurosciences. 2009;32(4):207–214. doi:10.1016/j.tins.2008.11.008.

22. Malnic B, Hirono J, Sato T, Buck LB. Combinatorial Receptor Codes for Odors. Cell. 1999;96(5):713–723. doi:10.1016/S0092-8674(00)80581-4.

23. Wilson CD, Serrano GO, Koulakov AA, Rinberg D. A primacy code for odor identity. Nature Communications. 2017;8(1):1477. doi:10.1038/s41467-017-01432-4.

24. Kepple DR, Giaffar H, Rinberg D, Koulakov AA. Deconstructing Odorant Identity via Primacy in Dual Networks. Neural Computation. 2019;31(4):710–737. doi:10.1162/neco_a_01175.

25. Niessing J, Friedrich RW. Olfactory pattern classification by discrete neuronal network states. Nature. 2010;465(7294):47–52. doi:10.1038/nature08961.

26. Ubeda-Bañon I, Saiz-Sanchez D, Flores-Cuadrado A, Rioja-Corroto E, Gonzalez-Rodriguez M, Villar-Conde S, et al. The human olfactory system in two proteinopathies: Alzheimer's and Parkinson's diseases. Transl Neurodegener. 2020;9(1):22. doi:10.1186/s40035-020-00200-7.

27. Kulkarni AS, del Mar Cortijo M, Roberts ER, Suggs TL, Stover HB, Pena-Bravo JI, et al. α-Synuclein perturbs ¡em¿in vivo¡/em¿ neural activity following seeding in the olfactory bulb. bioRxiv. 2020; p. 2020.04.17.045013. doi:10.1101/2020.04.17.045013.

28. Funabe S, Takao M, Saito Y, Hatsuta H, Sugiyama M, Ito S, et al. Neuropathologic analysis of Lewy-related alpha-synucleinopathy in olfactory mucosa. Neuropathology. 2013;33(1):47–58. doi:10.1111/j.1440-1789.2012.01329.x.

29. Ubeda-Bañon I, Saiz-Sanchez D, de la Rosa-Prieto C, Argandoña-Palacios L, Garcia-Muñozguren S, Martinez-Marcos A. α-Synucleinopathy in the human olfactory system in Parkinson's disease: involvement of calcium-binding protein- and substance P-positive cells. Acta Neuropathologica. 2010;119(6):723–735. doi:10.1007/s00401-010-0687-9.

30. Saito Y, Kawashima A, Ruberu NN, Fujiwara H, Koyama S, Sawabe M, et al. Accumulation of phosphorylated alpha-synuclein in aging human brain. Journal of Neuropathology and Experimental Neurology. 2003;62(6):644–654. doi:10.1093/jnen/62.6.644.

31. Roy S, Zhang B, Lee VMY, Trojanowski JQ. Axonal transport defects: a common theme in neurodegenerative diseases. Acta Neuropathologica. 2005;109(1):5–13. doi:10.1007/s00401-004-0952-x.

32. Lee HJ, Khoshaghideh F, Lee S, Lee SJ. Impairment of microtubule-dependent trafficking by overexpression of alpha-synuclein. European Journal of Neuroscience. 2006;24(11):3153–3162. doi:10.1111/j.1460-9568.2006.05210.x.

33. Perlson E, Maday S, Fu Mm, Moughamian AJ, Holzbaur ELF. Retrograde axonal transport: pathways to cell death? Trends in Neurosciences. 2010;33(7):335–344. doi:10.1016/j.tins.2010.03.006.

34. Choi WS, Palmiter RD, Xia Z. Loss of mitochondrial complex I activity potentiates dopamine neuron death induced by microtubule dysfunction in a Parkinson's disease model. Journal of Cell Biology. 2011;192(5):873–882. doi:10.1083/jcb.201009132.

35. Prots I, Veber V, Brey S, Campioni S, Buder K, Riek R, et al. alpha-Synuclein Oligomers Impair Neuronal Microtubule-Kinesin Interplay. Journal of Biological Chemistry. 2013;288(30):21742–21754. doi:10.1074/jbc.M113.451815.

36. Volpicelli-Daley LA, Gamble KL, Schultheiss CE, Riddle DM, West AB, Lee VMY. Formation of alpha-synuclein Lewy neurite-like aggregates in axons impedes the transport of distinct endosomes. Molecular Biology of the Cell. 2014;25(25):4010–4023. doi:10.1091/mbc.E14-02-0741.

37. Koscielnybunde E. EFFECT OF DAMAGE IN NEURAL NETWORKS. Journal of Statistical Physics. 1990;58(5-6):1257–1266. doi:10.1007/bf01026576.

38. Ruppin E, Reggia JA. PATTERNS OF FUNCTIONAL DAMAGE IN NEURAL-NETWORK MODELS OF ASSOCIATIVE MEMORY. Neural Computation. 1995;7(5):1105–1127. doi:10.1162/neco.1995.7.5.1105.

39. Horn D, Ruppin E. COMPENSATORY MECHANISMS IN AN ATTRACTOR NEURAL-NETWORK MODEL OF SCHIZOPHRENIA. Neural Computation. 1995;7(1):182–205. doi:10.1162/neco.1995.7.1.182.

40. Horn D, Levy N, Ruppin E. Neuronal-based synaptic compensation: A computational study in Alzheimer's disease. Neural Computation. 1996;8(6):1227–1243. doi:10.1162/neco.1996.8.6.1227.

41. Linster C. Computation in the Olfactory System. Computational Models of Brain and Behavior. 2017; p. 185–198. doi:doi:10.1002/9781119159193.ch14 10.1002/9781119159193.ch14.

42. Li Z, Hopfield JJ. Modeling the olfactory bulb and its neural oscillatory processings. Biol Cybern. 1989;61(5):379–92. doi:10.1007/BF00200803.

43. Brea JN, Kay LM, Kopell NJ. Biophysical model for gamma rhythms in the olfactory bulb via subthreshold oscillations. Proc Natl Acad Sci U S A. 2009;106(51):21954–9. doi:10.1073/pnas.0910964106.

44. Li G, Cleland TA. A coupled-oscillator model of olfactory bulb gamma oscillations. PLoS Comput Biol. 2017;13(11):e1005760. doi:10.1371/journal.pcbi.1005760.

45. Zavitz D, Youngstrom IA, Borisyuk A, Wachowiak M. Effect of interglomerular inhibitory networks on olfactory bulb odor representations. J Neurosci. 2020;doi:10.1523/JNEUROSCI.0233-20.2020.

46. Migliore M, Cavarretta F, Marasco A, Tulumello E, Hines ML, Shepherd GM. Synaptic clusters function as odor operators in the olfactory bulb. Proc Natl Acad Sci U S A. 2015;112(27):8499–504. doi:10.1073/pnas.1502513112.

47. Freeman WJ. Spatial properties of an EEG event in the olfactory bulb and cortex. Electroencephalography and Clinical Neurophysiology. 1978;44(5):586–605. doi:https://doi.org/10.1016/0013-4694(78)90126-8.

48. Virtanen P, Gommers R, Oliphant TE, Haberland M, Reddy T, Cournapeau D, et al. SciPy 1.0: fundamental algorithms for scientific computing in Python. Nat Methods. 2020;17(3):261–272. doi:10.1038/s41592-019-0686-2.

49. Cavarretta F, Burton SD, Igarashi KM, Shepherd GM, Hines ML, Migliore M. Parallel odor processing by mitral and middle tufted cells in the olfactory bulb. Sci Rep. 2018;8(1):7625. doi:10.1038/s41598-018-25740-x.

50. Osinski BL, Kay LM. Granule cell excitability regulates gamma and beta oscillations in a model of the olfactory bulb dendrodendritic microcircuit. J Neurophysiol. 2016;116(2):522–39. doi:10.1152/jn.00988.2015.

51. Desplats P, Lee HJ, Bae EJ, Patrick C, Rockenstein E, Crews L, et al. Inclusion formation and neuronal cell death through neuron-to-neuron transmission of alpha-synuclein. Proceedings of the National Academy of Sciences of the United States of America. 2009;106(31):13010–13015. doi:10.1073/pnas.0903691106.

52. Ubeda-Bañon I, Saiz-Sanchez D, de la Rosa-Prieto C, Martinez-Marcos A. α-Synuclein in the olfactory system in Parkinson's disease: role of neural connections on spreading pathology. Brain Structure and Function. 2014;219(5):1513–1526. doi:10.1007/s00429-013-0651-2.

53. Okuzumi A, Kurosawa M, Hatano T, Takanashi M, Nojiri S, Fukuhara T, et al. Rapid dissemination of alpha-synuclein seeds through neural circuits in an in-vivo prion-like seeding experiment. Acta Neuropathologica Communications. 2018;6(1):96. doi:10.1186/s40478-018-0587-0.

54. Longhena F, Faustini G, Missale C, Pizzi M, Spano P, Bellucci A. The Contribution of α-Synuclein Spreading to Parkinson's Disease Synaptopathy. Neural plasticity. 2017;2017:5012129–5012129. doi:10.1155/2017/5012129.

55. Chung HK, Ho HA, Pérez-Acuña D, Lee SJ. Modeling α-Synuclein Propagation with Preformed Fibril Injections. Journal of movement disorders. 2019;12(3):139–151. doi:10.14802/jmd.19046.

56. Lu XCM, Slotnick BM. Olfaction in rats with extensive lesions of the olfactory bulbs: implications for odor coding. Neuroscience. 1998;84(3):849–866. doi:https://doi.org/10.1016/S0306-4522(97)00520-4.

57. Neville KR, Haberly LB. Beta and Gamma Oscillations in the Olfactory System of the Urethane-Anesthetized Rat. Journal of Neurophysiology. 2003;90(6):3921–3930. doi:10.1152/jn.00475.2003.

58. Osinski BL, Kim A, Xiao W, Mehta NM, Kay LM. Pharmacological manipulation of the olfactory bulb modulates beta oscillations: testing model predictions. J Neurophysiol. 2018;120(3):1090–1106. doi:10.1152/jn.00090.2018.

59. Durante V, de Iure A, Loffredo V, Vaikath N, De Risi M, Paciotti S, et al. Alpha-synuclein targets GluN2A NMDA receptor subunit causing striatal synaptic dysfunction and visuospatial memory alteration. Brain. 2019;142(5):1365–1385. doi:10.1093/brain/awz065.

60. Cabin DE, Shimazu K, Murphy D, Cole NB, Gottschalk W, McIlwain KL, et al. Synaptic Vesicle Depletion Correlates with Attenuated Synaptic Responses to Prolonged Repetitive Stimulation in Mice Lacking α-Synuclein. The Journal of Neuroscience. 2002;22(20):8797. doi:10.1523/JNEUROSCI.22-20-08797.2002.

61. Wong YC, Krainc D. α-synuclein toxicity in neurodegeneration: mechanism and therapeutic strategies. Nature Medicine. 2017;23(2):1–13. doi:10.1038/nm.4269.

62. Volpicelli-Daley LA, Luk KC, Patel TP, Tanik SA, Riddle DM, Stieber A, et al. Exogenous α-synuclein fibrils induce Lewy body pathology leading to synaptic dysfunction and neuron death. Neuron. 2011;72(1):57–71. doi:10.1016/j.neuron.2011.08.033.

63. Calo L, Wegrzynowicz M, Santivañez-Perez J, Grazia Spillantini M. Synaptic failure and α-synuclein. Movement Disorders. 2016;31(2):169–177. doi:10.1002/mds.26479.

64. Schulz-Schaeffer WJ. Is Cell Death Primary or Secondary in the Pathophysiology of Idiopathic Parkinson's Disease? Biomolecules. 2015;5(3):1467–1479. doi:10.3390/biom5031467.

65. Iravani B, Arshamian A, Ohla K, Wilson DA, Lundströ M. Non-invasive recording from the human olfactory bulb. Nature Communications. 2020;11:648. doi:10.1038/s41467-020-14520-90.

66. David F, Courtiol E, Buonviso N, Fourcaud-Trocmé N. Competing Mechanisms of Gamma and Beta Oscillations in the Olfactory Bulb Based on Multimodal Inhibition of Mitral Cells Over a Respiratory Cycle. eNeuro. 2015;2(6). doi:10.1523/ENEURO.0018-15.2015.

67. Li Z. A model of the olfactory bulb and beyond [Dissertation]. California Institute of Technology; 1990. Available from: `https://resolver.caltech.edu/CaltechTHESIS:02192014-080819270`.

S1 Table. List of parameters and functions.

Table 1. The parameters are as given in [42]. Each sniff cycle runs for 395 ms, so $t_{final} = 395$.

$I_{b,i}$	0.243
$I_{c,i}$	0.1
α	0.15
$g_y(y_i)$	$\begin{cases} 2.86 + 2.86\tanh(\frac{y_i-1}{2.86}) & \text{if } y_i < 1 \\ 2.86 + .286\tanh(\frac{y_i-1}{.286}) & \text{if } y_i \geq 1 \end{cases}$
$g_x(x_i)$	$\begin{cases} 1.43 + 1.43\tanh(\frac{x_i-1}{1.43}) & \text{if } x_i < 1 \\ 1.43 + .143\tanh(\frac{x_i-1}{.143}) & \text{if } x_i \geq 1 \end{cases}$
$I_{odor,i}$	$\begin{cases} 0 & \text{if } t < 25 \\ 0.00429(t-25) & \text{if } 25 \leq t < 205 \\ 0.00429(t-25)e^{-0.03(t-205)} & \text{if } t \geq 205 \end{cases}$

S1 Fig. Effect of Flat Damage on Activity Pattern.

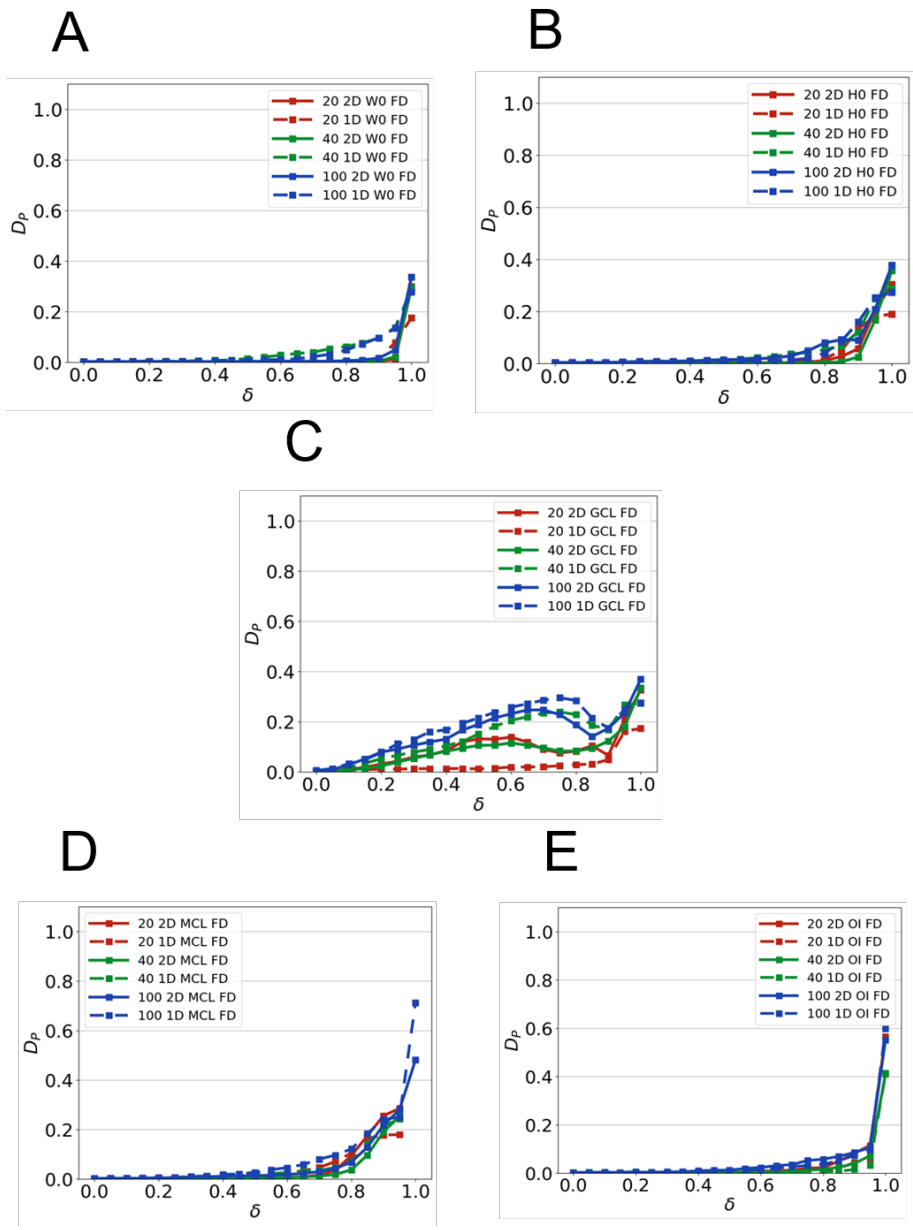

Distance in activity pattern (D_P) for flat damage to W_0 (A), H_0 (B), GCL (C), MCL (D), and OI (E) in every network architecture (20 units 1D, 20 units 2D, 40 units 1D, 40 units 2D, 100 units 1D, and 100 units 2D).

S2 Fig. Effect of Columnar Damage on Activity Pattern.

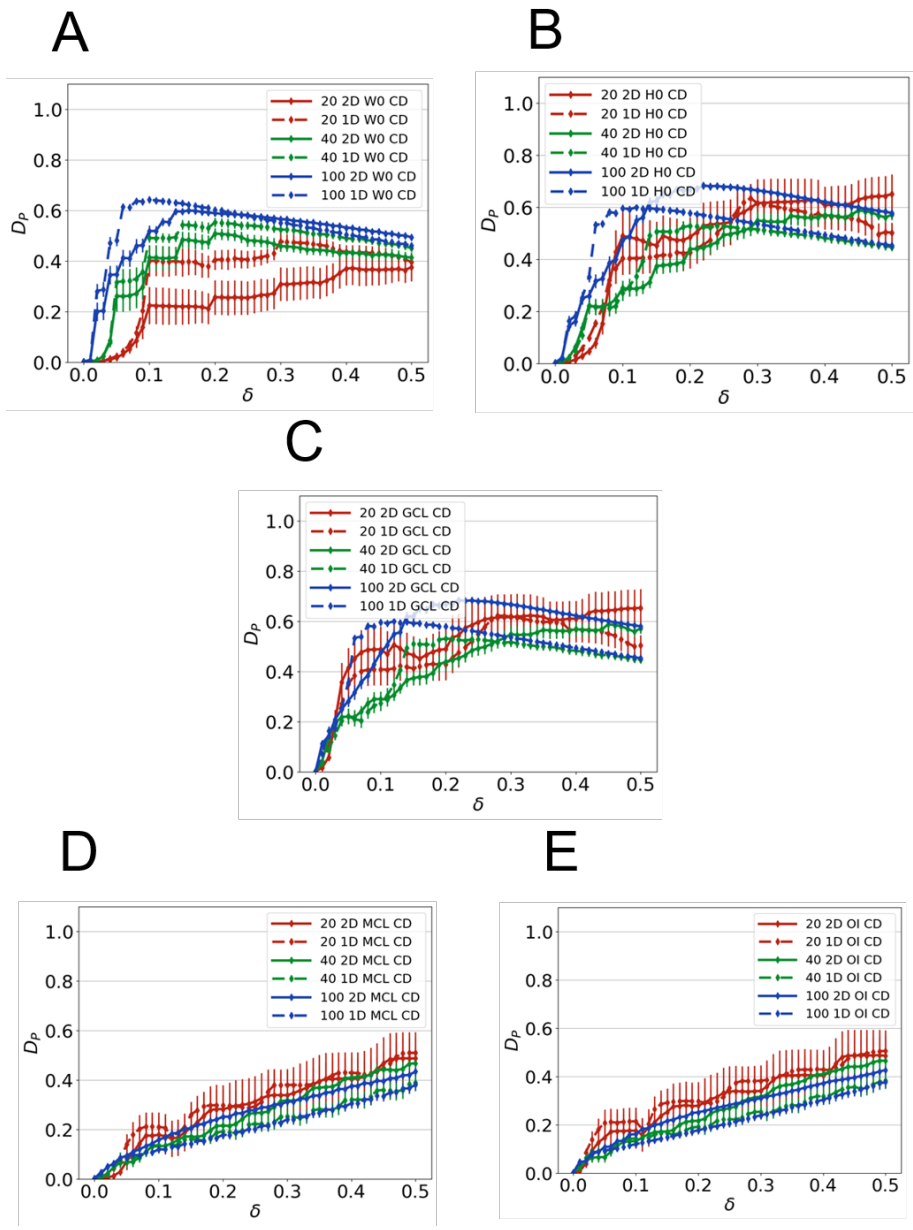

Distance in activity pattern (D_P) for columnar damage to W_0 (A), H_0 (B), GCL (C), MCL (D), and OI (E) in every network architecture (20 units 1D, 20 units 2D, 40 units 1D, 40 units 2D, 100 units 1D, and 100 units 2D).

S3 Fig. Effect of Seeded Damage on Activity Pattern.

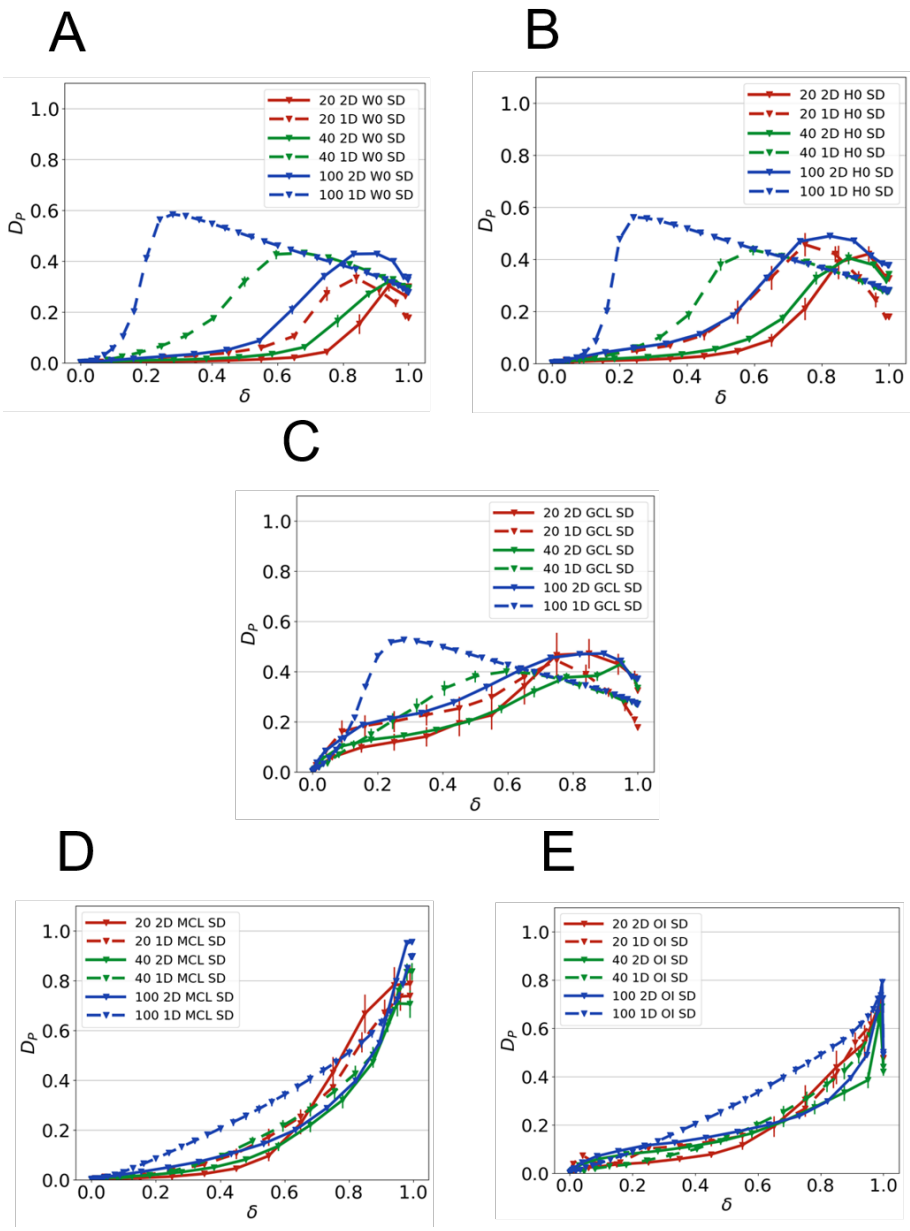

Distance in activity pattern (D_P) for seeded damage to W_0 (A), H_0 (B), GCL (C), MCL (D), and OI (E) in every network architecture (20 units 1D, 20 units 2D, 40 units 1D, 40 units 2D, 100 units 1D, and 100 units 2D).

S4 Fig. Effect of Flat Damage on Average Activity Level.

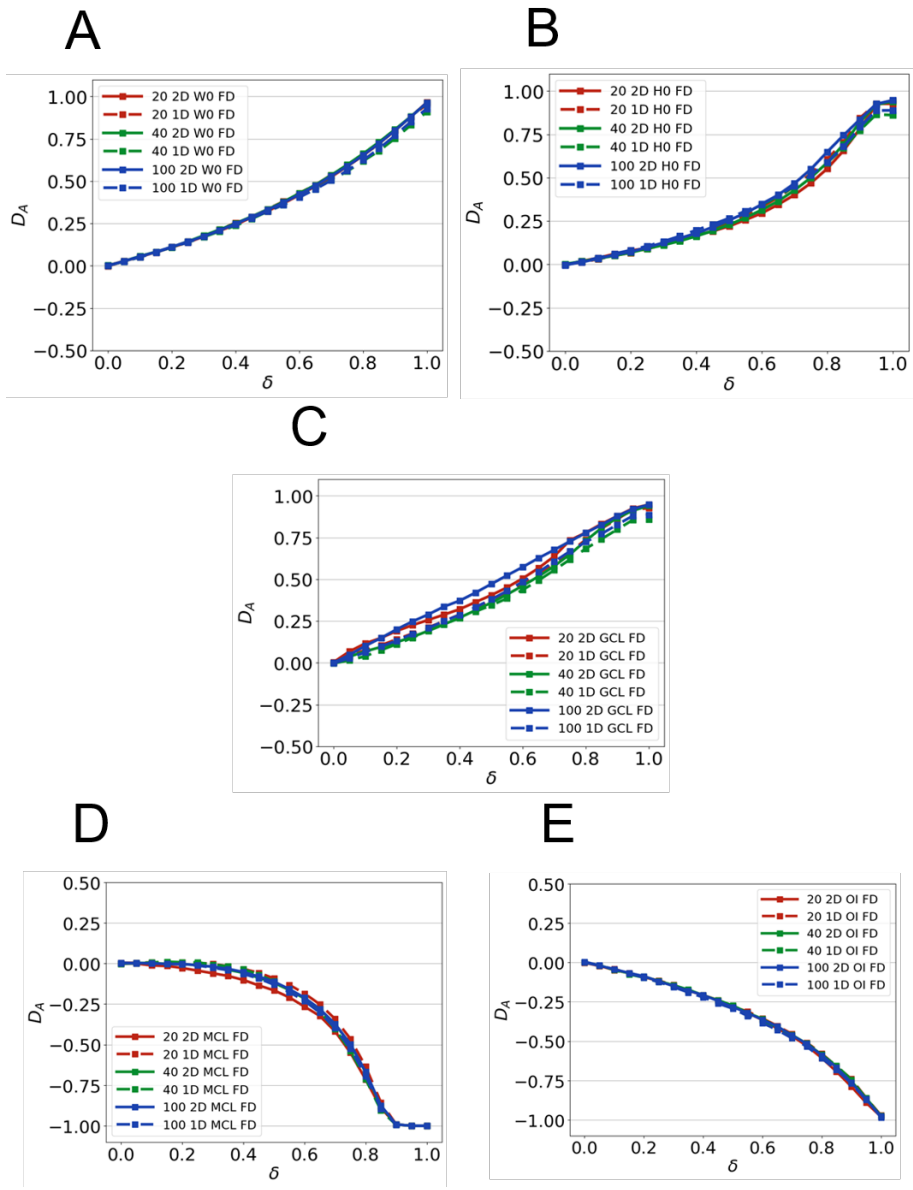

Distance in average activity level (D_A) for flat damage to W_0 (A), H_0 (B), GCL (C), MCL (D), and OI (E) in every network architecture (20 units 1D, 20 units 2D, 40 units 1D, 40 units 2D, 100 units 1D, and 100 units 2D).

S5 Fig. Effect of Columnar Damage on Average Activity Level.

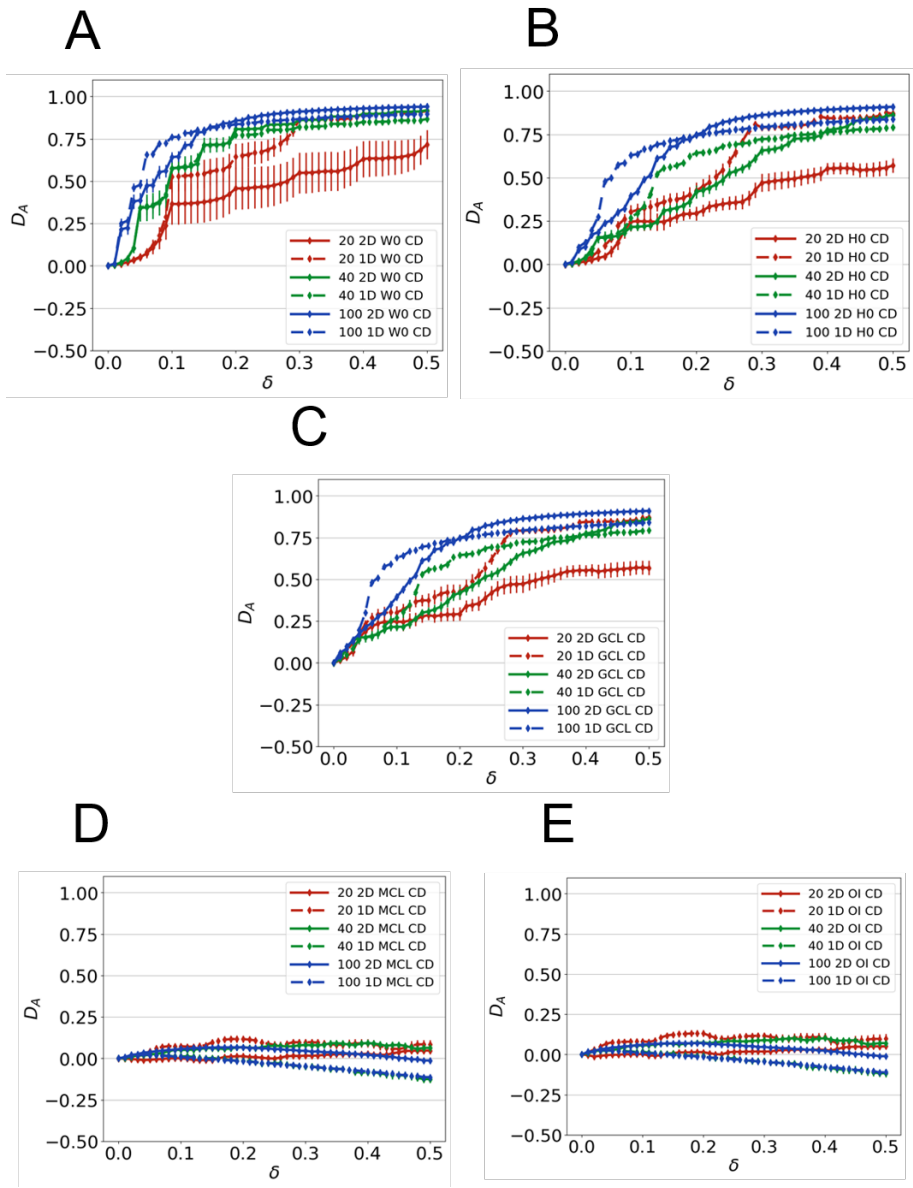

Distance in average activity level (D_A) for columnar damage to W_0 (A), H_0 (B), GCL (C), MCL (D), and OI (E) in every network architecture (20 units 1D, 20 units 2D, 40 units 1D, 40 units 2D, 100 units 1D, and 100 units 2D).

S6 Fig. Effect of Seeded Damage on Average Activity Level.

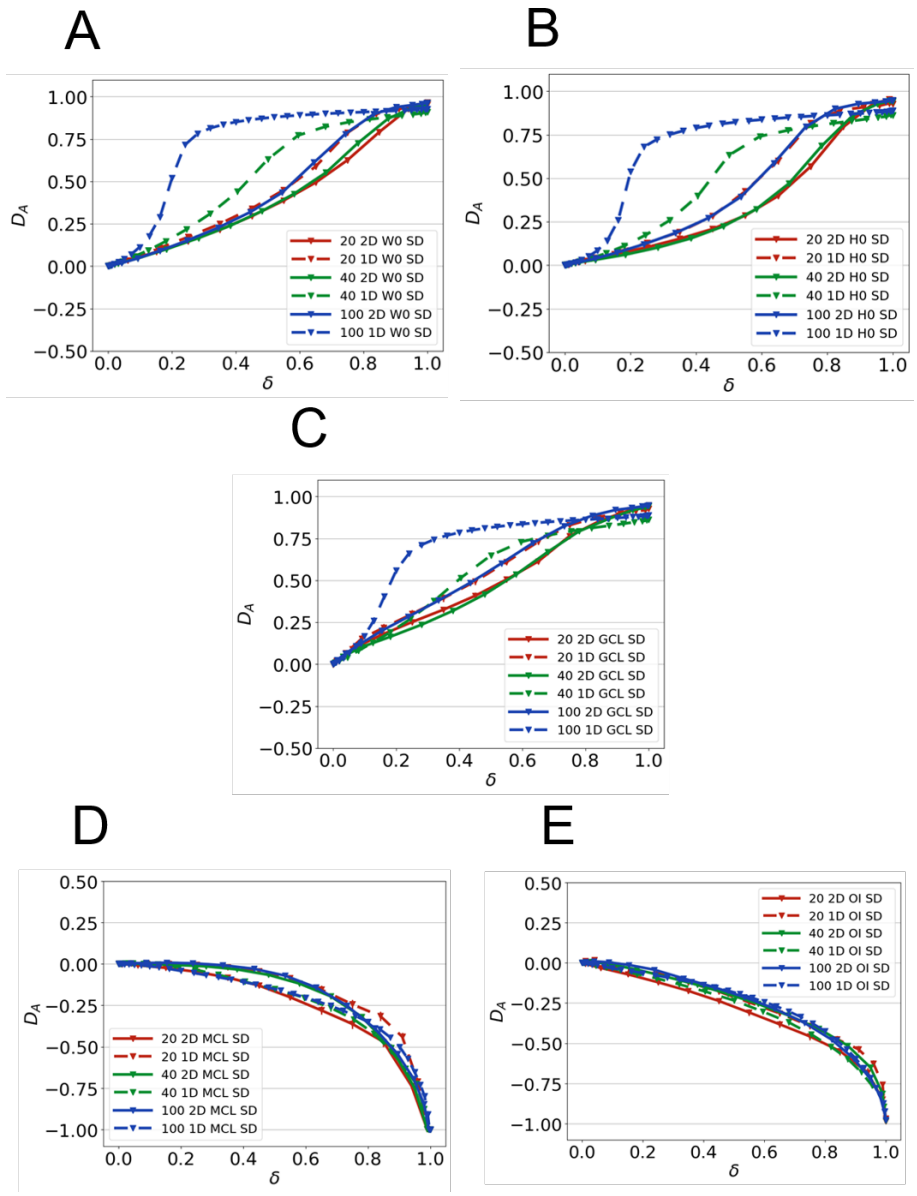

Distance in average activity level (D_A) for seeded damage to W_0 (A), H_0 (B), GCL (C), MCL (D), and OI (E) in every network architecture (20 units 1D, 20 units 2D, 40 units 1D, 40 units 2D, 100 units 1D, and 100 units 2D).

S7 Fig. Effect of Flat Damage on Oscillator Power.

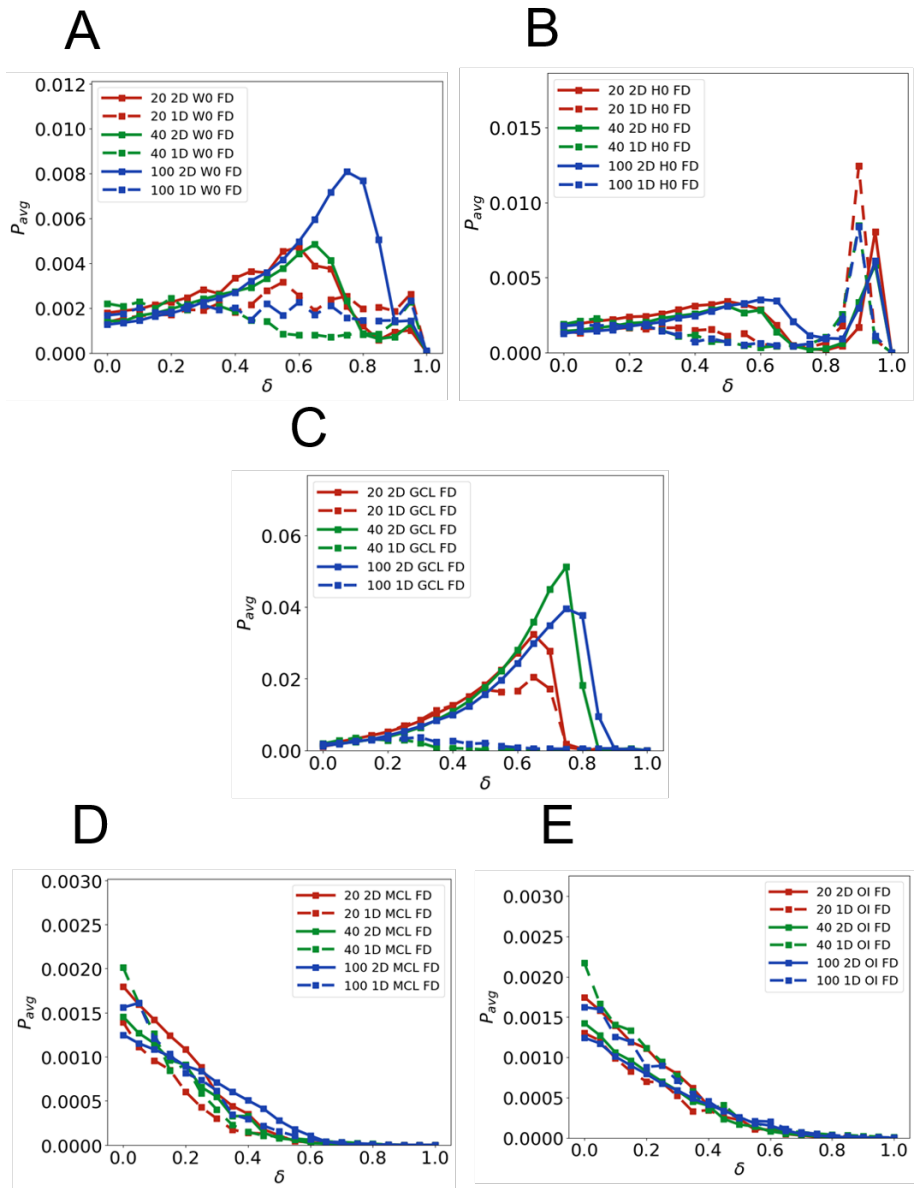

Average ocillatory power (P_{avg}) for flat damage to W_0 (A), H_0 (B), GCL (C), MCL (D), and OI (E) in every network architecture (20 units 1D, 20 units 2D, 40 units 1D, 40 units 2D, 100 units 1D, and 100 units 2D). Note the vertical axes do not have the same scale. Additionally, note that the 1D 20 unit network also experienced a rise in P_{avg} for damage to GCL, but this is likely because it was not truly 1D. The original Li-Hopfield network had extra connections, and the behavioral similarity to the 2D networks in some cases (including P_avg for seeded damage to W_0 and GCL, see S9 Fig) is likely due to this.

S8 Fig. Effect of Columnar Damage on Oscillatory Power.

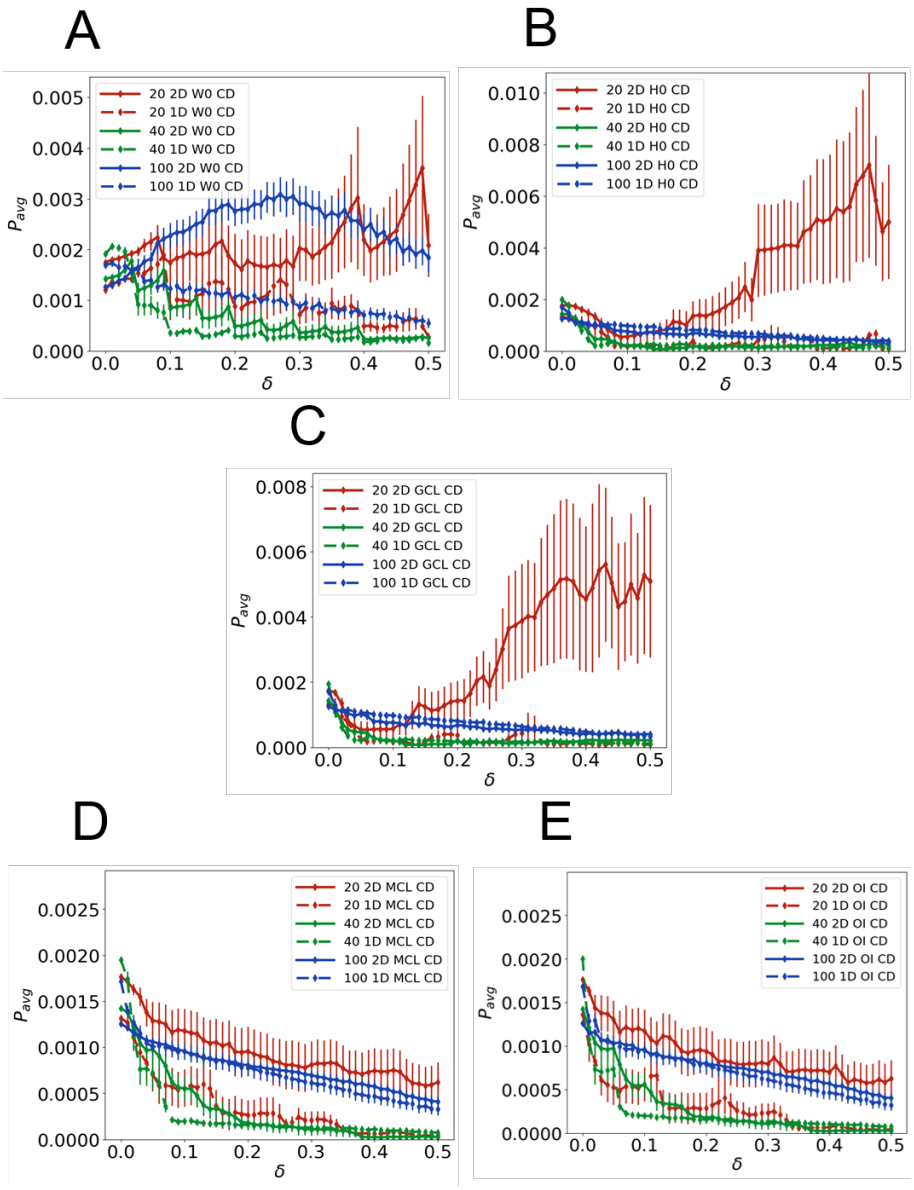

Average oscillatory power (P_{avg}) for columnar damage to W_0 (A), H_0 (B), GCL (C), MCL (D), and OI (E) in every network architecture (20 units 1D, 20 units 2D, 40 units 1D, 40 units 2D, 100 units 1D, and 100 units 2D). Note that the vertical axes do not all have the same scale.

S9 Fig. Effect of Seeded Damage on Oscillatory Power.

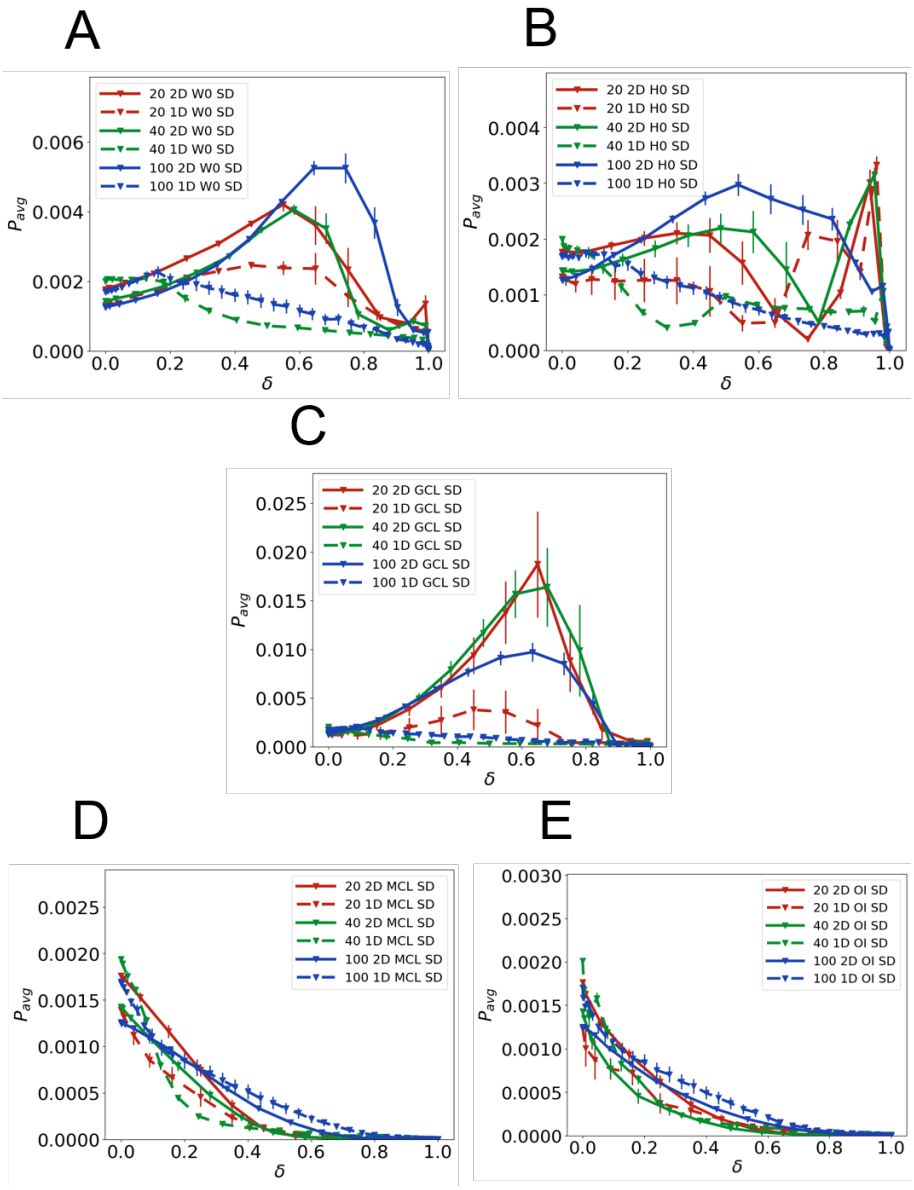

Average oscillatory power (P_{avg}) for seeded damage to W_0 (A), H_0 (B), GCL (C), MCL (D), and OI (E) in every network architecture (20 units 1D, 20 units 2D, 40 units 1D, 40 units 2D, 100 units 1D, and 100 units 2D). Note that not all the vertical axes had the same scale. The peak in P_{avg} occurred in all 2D networks for seeded damage to W_0, H_0, and GCL.

S10 Fig. Evolution of Cell Activity in Seeded Damage to W0 in the 2D 100 Unit Network

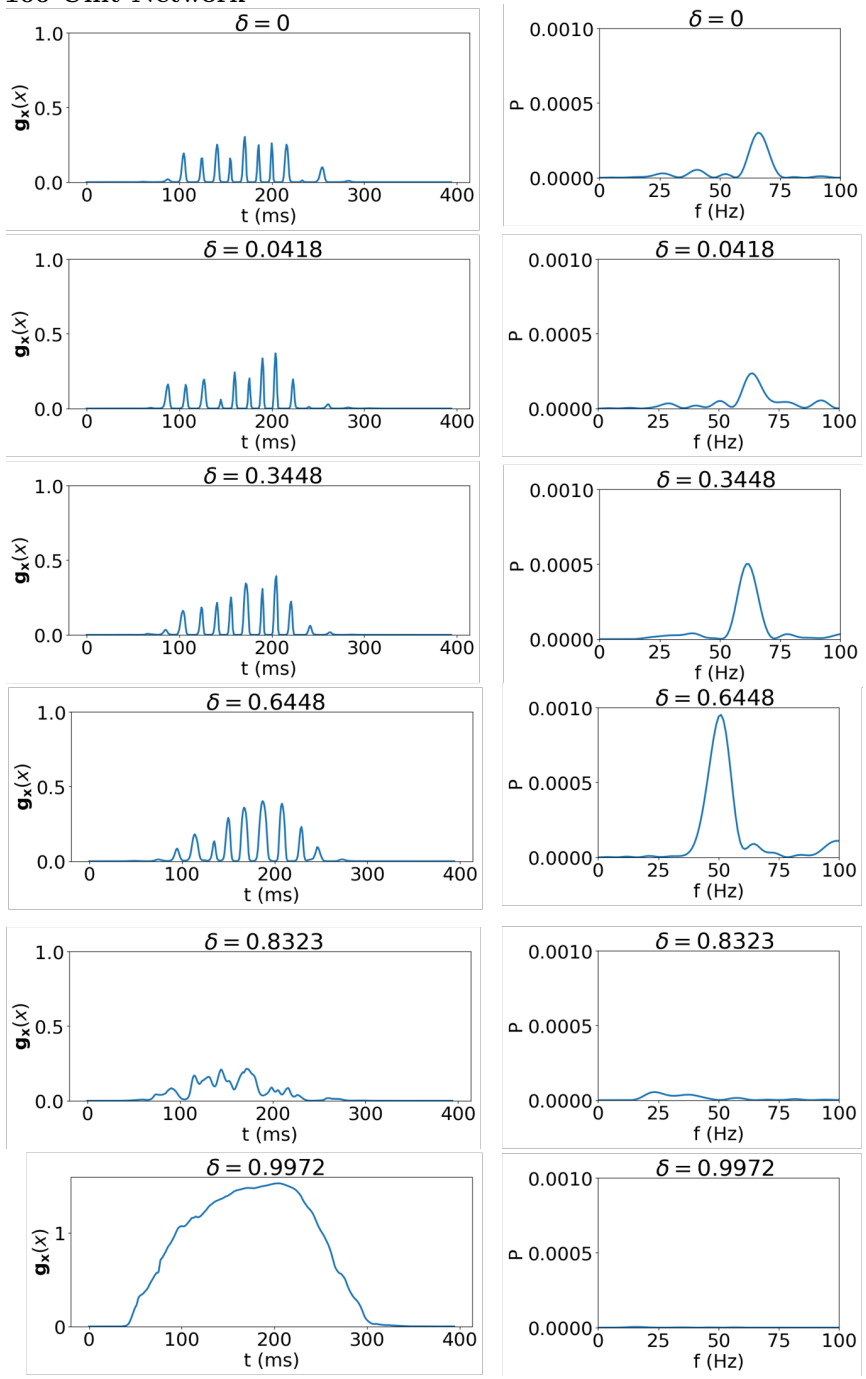

Cell activity ($\mathbf{g_x}$) at various levels of seeded damage to W0 in the 2D 100 unit network, with the associated power spectrum plotted next to each. The inhale peak is at 205 ms. The oscillation amplitude can be seen to grow from $\delta = 0$ to $\delta = 0.8448$, which is reflected clearly in the power spectra. Note that the vertical scale is larger in the last cell activity plot. The sharp fall in activity from about 225 ms to 300 ms can cause an increase in P_{avg}, but clearly is not actually an example of gamma band oscillatory behavior and is the reason for the shortened time window used for

calculating the power spectra for P_{avg}.

As stated in the text, the power spectrum was calculated from the cell activity high-pass filtered above 15 Hz from 125 ms to 250 ms. Some power density was present above 100 Hz, but power density below 100 Hz dominated the contribution to P_{avg}.

S11 Fig. Evolution of Cell Activity in Flat Damage to H0 in the 1D 100 Unit Network

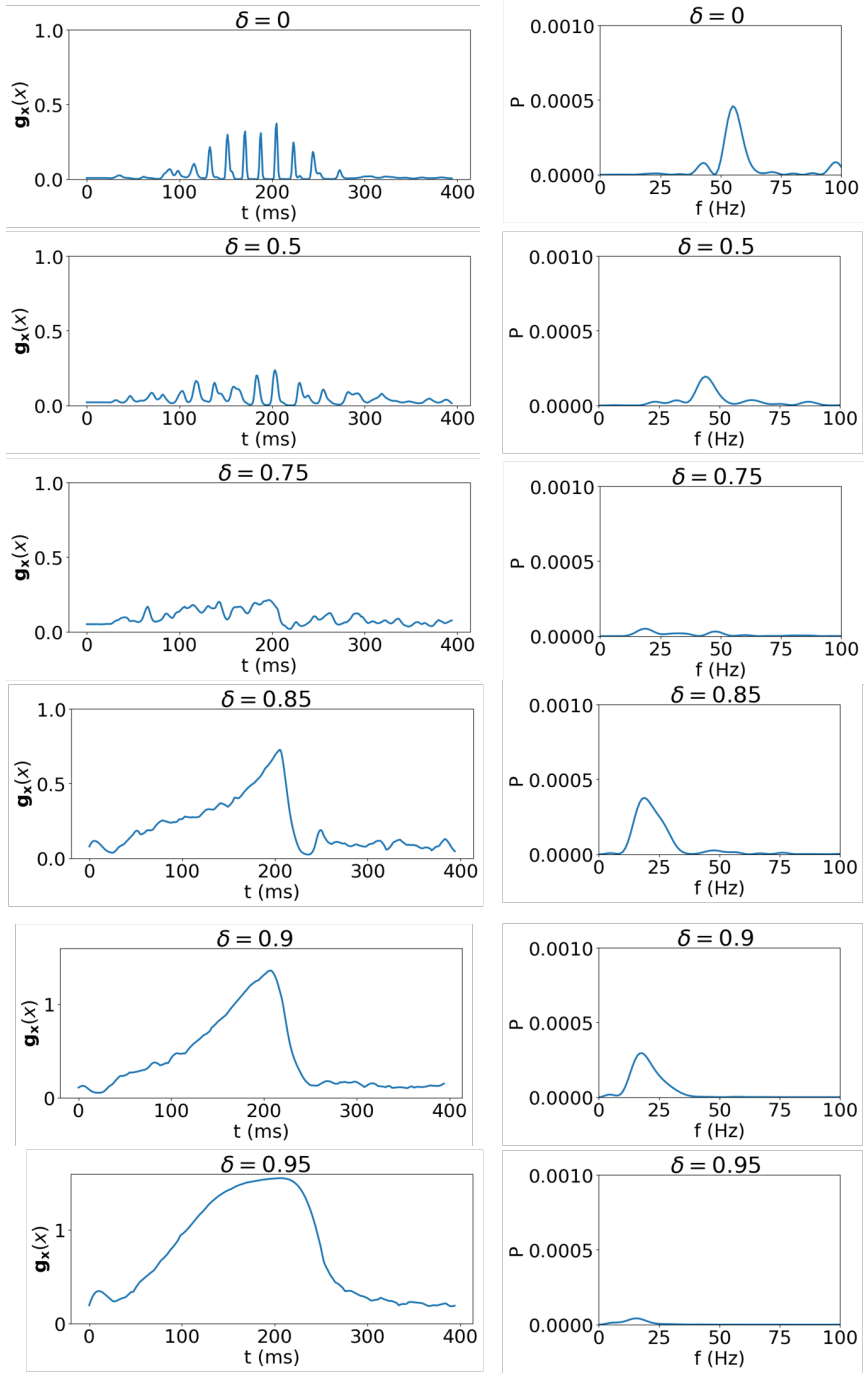

Cell activity ($\mathbf{g_x}$) at various levels of flat damage to H_0 in the 1D 100 unit network, with the associated power spectrum plotted next to each. The inhale peak is at 205 ms.

The cell activity changes little from $\delta = 0$ to $\delta = 0.5$. Note that the vertical scale is larger in the last two plots of cell activity. The sharp rise then drop seen in $\delta = 0.85$ and $\delta = 0.9$ is the cause of the spike in P_{avg} at the highest levels of damage for flat damage to H_0 in the 1D 100 unit network (see S7 FigB), and is an example of what causes the similar spikes in P_{avg} for flat damage to H0 in all networks (see S7 FigB), and for seeded damage to H0 in the 1D 20 unit, 2D 20 unit, and 2D 40 unit networks (see S9 Fig.

As stated in the text, the power spectrum was calculated from the cell activity high-pass filtered above 15 Hz from 125 ms to 250 ms. Some power density was present above 100 Hz, but power density below 100 Hz dominated the contribution to P_{avg}.